American Mineralogist, Volume 89, pages 327–338, 2004

Synthesis of beryllian sapphirine in the system MgO-BeO-Al_2O_3-SiO_2-H_2O and comparison with naturally occurring beryllian sapphirine and khmaralite, Part 2: A chemographic study of Be content as a function of *P*, *T*, assemblage and $FeMg_{-1}$ exchange

A. G. CHRISTY[1,*] AND E. S. GREW[2]

[1]Department of Applied Mathematics, Research School of Physical Sciences and Engineering, Australian National University, Canberra, ACT 0200, Australia

[2]Department of Earth Sciences, University of Maine, 5790 Bryand Research Center, Orono, Maine 04469-5790, U.S.A.

ABSTRACT

Beryllium is a significant constituent in sapphirine in some metamorphic and pegmatitic rocks, and thus could have a major effect on its stability relationships. Using the stoichiometries of reactions involving sapphirine and associated phases in the MgO-BeO-Al_2O_3-SiO_2 (MBeAS) system in conjunction with molar volume data, we have plotted maps of the sapphirine solid-solution field in both μ-μ and μ-*P* space, where μ is the chemical potential of an exchange component such as $(BeSi)(AlAl)_{-1}$. These maps give a pressure sequence of stable MBeAS univariant reactions and divariant assemblages that are consistent with experimental data, e.g., they show how Be stabilizes sapphirine + forsterite, which is rare in nature but readily synthesized over a wide *P*-*T* range in the presence of Be. We generate a MBeAS petrogenetic grid for sapphirine-bearing assemblages over the approximate range *T* = 700–900 °C, *P* = 0–2.5 GPa, identify divariant and univariant assemblages containing sapphirine with maximum Be, and determine the sense of variation of maximum Be content with *P*. At lower *T*, maximum Be occurs at the low-*P* limit of surinamite stability, ca. 0.5 GPa. At higher *T*, maximum Be increases with *P*, following the MBeAS univariant reactions involving (sapphirine + surinamite + orthopyroxene + chrysoberyl + forsterite or spinel).

Natural assemblages containing sapphirine and its Be-rich near-analog khmaralite from the Napier Complex, Enderby Land, East Antarctica formed at higher *T* (900–1100 °C) than the experiments and in bulk compositions containing substantial Fe. Associated minerals include garnet, sillimanite, quartz, and magnesiotaaffeite-6*N*'3*S* ("musgravite"), whereas forsterite is absent and cordierite is a local, late phase. $\mu_{(BeSi)(AlAl)-1}$-μ_{FeMg-1} diagrams show that the stability of magnesiotaaffeite-6*N*'3*S* causes the maximally beryllian khmaralite to shift from a magnesian composition in equilibrium with orthopyroxene + surinamite + forsterite + chrysoberyl, as in the MBeAS subsystem, to a more Fe-rich composition associated with garnet + surinamite + magnesiotaaffeite-6*N*'3*S* + chrysoberyl. Khmaralite associated with sillimanite + garnet + surinamite + magnesiotaaffeite-6*N*'3*S* or chrysoberyl in a Napier Complex pegmatite from Khmara Bay is predicted to be the most Be-rich possible in the presence of sillimanite, whereas the sillimanite + quartz ± orthopyroxene ± garnet associations in quartz granulites requires a sapphirine much lower in both Be and Fe; analyses are roughly in accord with these predictions. The shape of the sapphirine/khmaralite solid-solution field is such that there is a positive correlation between high Be and high Fe^{2+}, a chemographic effect independent of any crystal chemical effects due to the clustering of Fe and Be in the crystal structure of khmaralite.

The diagram for FMBeAS shows that sapphirine + quartz, which is often cited as evidence for ultrahigh temperatures (e.g., ≥ 1040 °C), is stabilized to lower *T* and higher *P* than in the corresponding Be-free system. Hence, this minimum *T* may be valid only in rocks with relatively abundant sapphirine and/or very low bulk Be content so that what Be is present in the system is not concentrated in sapphirine.

INTRODUCTION

In the first part of this study (Christy et al. 2002), we reported the synthesis and characterization of beryllian sapphirine-2*M* in the MgO-BeO-Al_2O_3-SiO_2-H_2O (MBeASH) system with up to 1.0 Be per 20 oxygen atoms. This value is significantly higher than the maximum value of 0.78 Be per formula unit observed in natural khmaralite associated with magnesiotaaffeite-6*N*'3*S*, sillimanite, and garnet (Grew et al. 2000; Barbier et al. 2002). The distinction between beryllian sapphirine and khmaralite is subtle: partial ordering of Be into the more polymerized tetrahedral sites brings about a doubling of the unit cell in the latter (Christy 1988a; Barbier et al. 1999). This ordering could have resulted from annealing following crystallization, i.e., khmaralite could have originally crystallized with the same degree of cation order as Be-poor sapphirine and synthetic beryllian sapphirine (Christy et al. 2002). There is no discernible break in composition between khmaralite and a Be-free sapphirine near $(Mg, Fe)_{3.5}Al_9Si_{1.5}O_{20}$,

* Current Address: Department of Geology, Building 47, Australian National University, Canberra, ACT 0200, Australia. E-mail: andyc@geology.anu.edu.au

and the cation ordering responsible for the superstructure appears to develop gradually with increasing Be content (Grew et al. 2000; Grew 2002; Grew et al. in preparation). Hence, in the present paper, "sapphirine" and "sapphirine/khmaralite" (abbreviated to "Spr" and "Spr/Khm", Table 1) are used interchangeably for sapphirine-series minerals with variable Be content.

Christy et al. (2002) hypothesized that the relatively low Be content of natural khmaralite was due to its Fe content and relatively aluminous bulk composition of the natural matrix, so we decided to investigate further the relationship between the extent of $(BeSi)(AlAl)_{-1}$ substitution in Spr/Khm and the identity and chemistry of the associated phases. Our interest in phase equilibria involving Spr/Khm was further stimulated by the apparent stability of beryllian sapphirine with surinamite + forsterite + chrysoberyl up to $T = 900$ °C, $P = 1.3$ GPa in the synthetic MBeASH system (Christy et al. 2002). Be-free sapphirine and forsterite have at most a very small field of compatibility in MAS, confined to $T << 800$ °C and $P < 0.5$ GPa under very dry conditions (Grew et al. 1994). Incorporation of Be into sapphirine evidently extends the field of mutual stability of these minerals over a much wider range of pressure and temperature.

The first objective of the present paper is to develop a novel approach related to those of Korzhinsky (1959) and Thompson (1979) for constructing plots in chemical potential space of the sapphirine solid solution field partitioned into subfields for each of its associated phases. These diagrams are used to investigate the effect of Be content on the stability fields of assemblages containing Spr, and their evolution as a function of pressure. A succession of stable MBeAS univariant lines is predicted, compatible with those evidenced experimentally, which allows construction of a partial MBeAS petrogenetic grid covering the *P-T* range of the synthetic experiments of Christy et al. (2002). The chemographic treatment of this study is applied further to identify assemblages containing Spr/Khm with highest Be content as a function of *P* and *T*, and the sense of variation of maximum Be with pressure determined for divariant and univariant assemblages.

Calculation of equilibria in the MBeAS system is hampered by the paucity of available data for Be-bearing phases. In general, enthalpies of formation, entropies, and heat capacities are not known for these minerals. However, molar volume data is now available for all phases of interest, including Be-bearing sapphirine solid solutions (Christy et al. 2002). Volume changes therefore may be calculated for balanced reactions involving phases of given composition. For a univariant reaction involving five distinct phases in the MBeAS system, this allows the high-pressure side of the equilibrium to be identified. If the composition of a solid solution is replaced in the equation by the composition of the corresponding exchange vector, then the sense of pressure variation of the phase composition may be calculated. It is also possible to ascertain the pressure variation of the amount of an exchange component such as $(BeSi)(AlAl)_{-1}$ or $(AlAl)(MgSi)_{-1}$ in a specified phase in an assemblage of higher variance.

The second objective is to apply this approach to natural assemblages where Fe is pervasive. Thus, the chemographic approach is extended in the final section of this paper to the five-component system including FeO (FMBeAS) involving the additional phases sillimanite, quartz and magnesiotaaffeite-6*N*'3*S*. We have selected the Napier Complex, Enderby Land, Antarctica to test our approach; this granulite-facies complex is one of the few natural systems known to contain Be in sufficient quantities to be petrologically significant and yet be amenable for modeling by the relatively simple FMBeAS system. The approach demonstrates its utility for clearly depicting the relationship between assemblage and composition of the Spr/Khm, locating the assemblages containing maximum Be, and the interaction between Fe and Be content of Spr/Khm.

Associated phases

Abbreviations and end-member compositions for MBeAS associates of Spr/Khm that are considered in this study are given

Table 1. Molar volumes of MBeAS end-members

	Symbol§		V / cm^{3}mol^{-1}	Reference
Sapphirine	Spr	$Mg_4Al_8Si_2O_{20}$	198.76	*
Sapphirine	Spr	$Mg_{3.5}Al_9Si_{1.5}O_{20}$	198.47	†
Sapphirine	Spr	$Mg_4Al_6BeSi_3O_{20}$	193.48	*
Surinamite	Sur	$Mg_3Al_4BeSi_3O_{16}$	152.14	Hölscher et al. (1986)
Spinel	Spl	$MgAl_2O_4$	39.26	‖
Chrysoberyl	Cb	$BeAl_2O_4$	34.24	Hazen and Finger (1987)
Magnesiotaaffeite-6*N*'3*S*	Mtf	$Mg_2Al_6BeO_{12}$	115.44	‡
Corundum	Crn	Al_2O_3	25.24	‖
Forsterite	Fo	Mg_2SiO_4	43.09	‖
Enstatite	Opx	$Mg_2Si_2O_6$	61.80	‖
Mg-Tschermak	Opx	$MgAl_2SiO_6$	58.13	‖
Pyrope	Grt	$Mg_3Al_2Si_3O_{12}$	111.70	‖
Sillimanite	Sil	Al_2SiO_5	49.21	‖
Cordierite	Crd	$Mg_2Al_4Si_5O_{18}$	230.16	‖
Be-Cordierite	BeCrd	$Mg_2Al_2BeSi_6O_{18}$	221.90	#
Beryl	Brl	$Al_2Be_3Si_6O_{18}$	203.19	**
Phenakite	Phn	Be_2SiO_4	37.17	††
Quartz	Qtz	SiO_2	22.39	‖

* Linear fit to data, Christy et al. (2002).
† Extrapolated from sample B, Christy et al. (2002).
‡Extrapolated from data of Nuber and Schmetzer (1983).
§ Symbols based on Kretz (1983) and consistent with Baba et al. (2000).
‖ Holland and Powell (1998).
Hölscher and Schreyer (1989).
** Hazen et al. (1986).

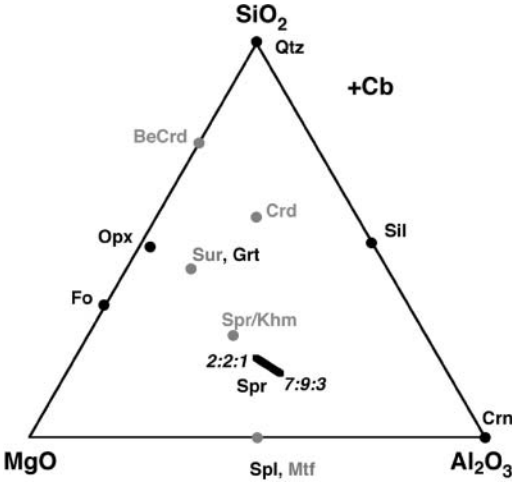

Figure 1. Compositions used for calculations on MBeAS phases (Tables 1 and 4), projected into the MAS triangle from chrysoberyl (Cb). Be-free Spr solid-solution line is also shown for comparison. Compositions containing Be are indicated in gray, Be-free compositions in black.

in Table 1, along with molar volumes, which are discussed below. Compositions are depicted in Figure 1, projected onto the MAS triangle from Cb. Solid solution in the variable-composition phases is shown in Figure 7 of Christy et al. (2002).

Phases lacking essential Be that are included in the study are Opx, Grt, Sil, Spl, Qtz, Crn, and Fo. All but Fo were observed, though not necessarily in mutual equilibrium, with Spr/Khm in pegmatites and their quartz granulite hosts of the Napier Complex (Grew 1981, 1998; Grew et al. 2000 and in preparation). Forsterite is included because the experimental data of Christy et al. (2002) suggest coexistence with Spr/Khm over a much broader range in the Be-bearing system than the restricted stability field that Grew et al. (1994) estimated to be at $P < 0.4$ GPa, T << 800 °C in MAS. Beryllium is not expected to play a role in the stability of any of these phases. In the Napier Complex their Be content rarely exceeds 30 ppm, the maximum being 140 ppm in B-bearing sillimanite in association with khmaralite (Grew 2002; Grew et al. in preparation). Incorporation of Be in Fo is limited, less than in associated Opx (Hörmann 1966; Brenan et al. 1998)

The presence of Be in the system brings three Be phases into association with Spr/Khm, all which are included in the calculations. Surinamite features prominently in the reactions considered in this study as it is the prevalent Be-rich breakdown product of sapphirine in both natural and synthetic systems. Chrysoberyl was included as it appears as a Be sink in the syntheses of Hölscher et al. (1986) and Hölscher (1987), and was deduced to be an associate of maximally beryllian Spr/Khm over a wide range of *P* and *T*. Chrysoberyl is also found in the khmaralite-bearing pegmatite at "Zircon Point" (Grew 1981, 1998). Magnesiotaaffeite-6*N*'3*S* (formerly "musgravite," see Armbruster 2002) — $(MgAl_7)(Mg_2BeAl)O_{16}$, equivalent to spinel + chrysoberyl — is another Be oxide occurring with Spr/Khm (Grew 1981, 1998; Grew et al. 2000); it also appeared in one of Hölscher's syntheses at low *P* and high *T* (0.1 GPa, 1200 °C).

Cordierite has been included in the calculation. It can incorporate Be in the synthetic MBeAS system, and the hexagonal end-member $Mg_2Al_2BeSi_6O_{18}$ ("BeCrd") is stable over an extensive *P-T* range (Hölscher and Schreyer 1989). However, there is a wide solvus gap between Crd and BeCrd at petrogenetically relevant temperatures. Orthorhombic Crd apparently incorporates less than 0.125 Be per formula unit (p.f.u) at temperatures from 850 °C to 1400 °C, whereas the minimum Be content of BeCrd is ca. 0.65 p.f.u. at 1100 °C and 0.72 p.f.u. at 800 °C. The solvus line for Crd-BeCrd proposed by Hölscher and Schreyer (1989) suggests that the beryllian cordierite composition with $^2/_3$ Be p.f.u is stable above ca. 1000 °C. This composition is coplanar in the MBeAS tetrahedron with the assemblage Sur + Qtz + Cb, although there is at present no evidence for a stable reaction BeCrd + Crd → Sur + Qtz + Cb. Beryllian cordierite has neither been found to date in natural assemblages, nor been demonstrated to be a component of any natural cordierite. Up to 0.44–0.48 Be p.f.u has been reported in natural cordierite, but this is almost invariably incorporated via the substitution $(Na,K,Ca_{0.5})BeAl_{-1}$ (e.g., Černý and Povondra 1966; Piyar et al. 1968; Povondra et al. 1984; Grew et al. 2000; Grew 2002). Cordierite reported by Baba et al. (2000) could be a rare exception in which this substitution accounts for only half of the inferred, but not measured, Be content of 0.24 Be per formula unit, i.e., 0.12 Be could be incorporated via the $(BeSi)(AlAl)_{-1}$ substitution that relates Crd to BeCrd.

MAS PETROGENETIC GRID

An approximately quantitative petrogenetic grid for all 9 phases in the MAS system is shown in Figure 2. The grid has been extrapolated from the quartz-absent grid of Hensen (1987) to accommodate quartz-bearing assemblages by allowing the reaction Opx + Sil → Spr + Qtz of Chatterjee and Schreyer (1972) and Crd → Opx + Sil + Qtz to intersect, thus generating a new Qtz-present, Crn- and Grt-absent invariant point. A difference from the grid of Christy (1988b) is a set of new invariant points at $P < 0.5$ GPa, $T < 800$ °C, which are required to produce a small stability field for Spr + Fo. One of these invariant points is [Chl] of Grew et al. (1994). The other points arise unambiguously as a consequence of the need to connect this point in a self-consistent fashion with the $T > 800$ °C portion of the grid. Note that the results of Seifert (1974) indicate that the univariant reactions Opx + Spr → Crd + Spl and Opx + Spl → Crd + Fo shift to lower pressures with increasing *T*, and are expected to be curved in *P-T* space due to variations in the Al content of the pyroxene (cf., Hensen 1987). Few data are available for MBeAS univariant reactions at present, except that Hölscher et al. (1986) approximately located the low-pressure breakdown reaction of surinamite, Sur → Opx + Spr + Crd + Cb as being nearly isobaric and at about 0.5 GPa at $T > 800$ °C (Fig. 2). The high-*P* stability limit of Sur is determined by the reaction (Sur → Grt + Cb), which occurs at $P = 4.3$–4.7 GPa at 700–1000 °C (Hölscher et

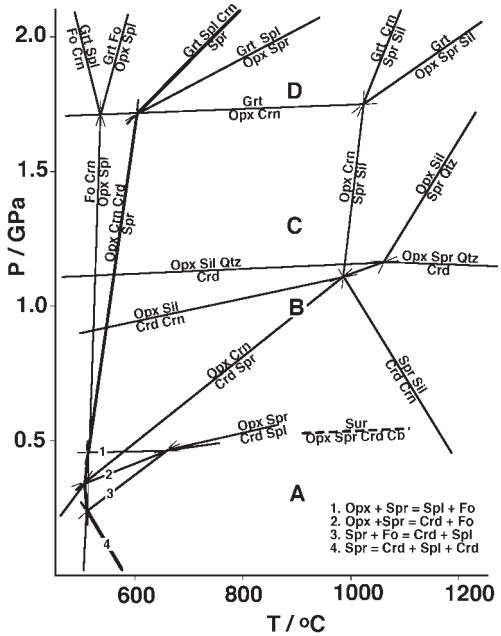

FIGURE 2. Semi-quantitative petrogenetic grid for MAS system constructed by combining portions of the grids in Hensen (1987), Christy (1988b), and Grew et al. (1994). Univariant lines defining Spr stability shown in bold. Approximate position of MBeAS univariant reaction defining low-P stability limit of Sur shown dashed (from Hölscher et al. 1986). Letters A-D indicate *P-T* conditions for Figures 4a–d. Numbers 1–4 identify low-*P*, low-*T* univariant reactions listed at bottom right.

al. 1986). This pressure is much higher than the 2.0–2.5 GPa at which Spr breakdown occurs over the same temperature range in MAS via the reaction Spr → Grt + Crn + Spl (Fig. 2). Clearly, Sur is a high-Be, high-Si associate of Spr/Khm throughout the higher-pressure part of the Spr/Khm stability field.

The work on synthetic Sur, Spr, and BeCrd by Hölscher et al. (1986), Hölscher (1987), and Hölscher and Schreyer (1989) implies that Cb is a stable high-Be, low-Si associate throughout much of the stability field of Spr/Khm. Consideration of molar volumes indicates that Mtf is likely to be unstable at high P with respect to (Cb + Spl) (see below). Magnesiotaaffeite does not seem to be stable in experiments on the synthetic MBAS system at $T < 1200$ °C (Christy et al. 2002). However, the occurrence of Mtf in preference to Cb in one 1200 °C synthetic run and also in the high-temperature natural assemblages of the Napier Complex (Grew 1981, 1998; Grew et al. 2000) suggests that high temperature may broaden the Mtf stability field. Magnesiotaaffeite associated with Spr/Khm in the Napier Complex contains substantial Fe^{2+} and Zn, which are expected to favor Mtf over Cb because the latter incorporates little of either impurity.

Some constraints on the MBeAS univariant reaction(s) limiting the stability of Spr/Khm at high pressure can be identified through consideration of the experimental data and the relationships shown in Figures 1 and 2. The only Spr-out reaction chemographically consistent with the divariant assemblage Spr + Sur + Cb + Fo, known to be stable at 900 °C and 1.3–2.0 GPa (Christy et al. 2002), is Spr → Sur + Cb + Fo + Crn. However, Crn is only stable with Fo at lower temperatures (Fig. 2). At 800 –900 °C, the univariant reaction that terminates the stability of Spr/Khm at high P must involve Spl rather than Fo. The model presented below identifies the reaction as Spr → Sur + Spl + Grt + Crn (Table 2), which implies the existence of several univariant reactions at $P > 2.0$ GPa but below the ultimate limit of Spr/Khm stability. In general, consideration of possible reaction stoichiometries and calculated volume changes along an isotherm allows us to interpolate, order, and locate approximately several more MBeAS reactions between ambient and the high-P limit that are extremely likely to be stable. These reactions can be used to construct a grid for the MBeAS system over a range of P and T (see below).

Molar volume data

The ΔV estimates are calculated from molar volumes obtained at room temperature, 1 atm pressure. Because the equilibria considered are fluid-absent, all solid bulk moduli are on the order of 100 GPa, and thermal expansivities are on the order of 10^{-5}/K (Hazen and Finger 1982), compression over the pressure range 1 bar^{-1} GPa is almost exactly compensated by expansion over the range 0–1000 °C. Therefore, ambient molar volumes and particularly molar volume *differences* provide a fair estimate of those applying near 1 GPa, 1000 °C.

Molar volumes for MBeAS end-member compositions are presented in Table 1, with units converted from the original source values where necessary. Where appropriate, molar volumes are given in Table 3 for the exchange components $(AlAl)(MgSi)_{-1}$, $(BeSi)(AlAl)_{-1}$, and $FeMg_{-1}$ in Spr/Khm or other specified phases. Molar volumes for solid solutions used in volume calculations of this study are given in Table 4.

For consistency with the data for synthetic Fe-free beryllian sapphirine and surinamite, the Be-free sapphirine data of Christy et al. (2002) are used. It should be noted that these volumes are slightly larger than those of either the sapphirine from the type locality used for the original structure solution (Moore, 1969: 197.5 ± 3 cm^3/mol) or the fitted thermodynamic data set values [196.10 cm^3/mol for the 2:2:1 composition and 195.16 cm^3/mol for 7:9:3 in Holland and Powell (1998)]. The reason for the discrepancy is not clear, but cation disorder may be responsible. Good agreement is observed with the molar volume of 199.1 ± 1 cm^3/mol calculated for the synthetic 2:2:1 sapphirine of Seifert (1974).

Molar volumes of magnesiotaaffeite-6N'3S, $(Mg,Fe,Zn)_2Al_6BeO_{12}$, and its polysomatic relative magnesiotaaffeite-2N'2S, formerly "taaffeite" (see Armbruster 2002), $(Mg,Fe,Zn)_3Al_8BeO_{16}$, were derived from the unit-cell parameters of Nuber and Schmetzer (1983). These authors give data for one magnesiotaaffeite-2N'2S and two magnesiotaaffeite-6N'3S with Mg:Fe:Zn contents of 2:81:0.15:0.04, 1.63:0.37:0.00, and 1.13:0.59:0.28 respectively. The unit-strength M-O bond lengths for Mg, Fe and Zn are respectively 1.693, 1.734, and 1.704 Å (Brese and O'Keeffe 1991), implying that the cell parameter increase due to

Table 2. Molar volumes of exchange components

Phase		V (cm^3/mol)	Reference
Spr*	$(BeSi)(AlAl)_{-1}$	–5.28	†
Spr*	$(AlAl)(MgSi)_{-1}$	–0.58	†
Spr*	$FeMg_{-1}$	1.29	§
Opx	$(AlAl)(MgSi)_{-1}$	–3.67	†
Opx	$FeMg_{-1}$	1.63	§
Grt	$FeMg_{-1}$	0.64	§
Spl	$FeMg_{-1}$	0.96	§
Crd	$(NaBe)Al_{-1}$	–3.40	‡
Crd	$(BeSi)(AlAl)_{-1}$	–8.26	†
Crd	$(AlAl)(MgSi)_{-1}$	–1.09	‖
Crd	$FeMg_{-1}$	1.92	§

* Data for Sur and Khm assumed to be same as for Spr.
† Subtraction of data in Table 3, Christy et al. (2002).
‡ See text.
§ Subtraction, data of Holland and Powell (1998).
‖ Calculated from cell volumes of Table 1.

Table 3. Molar volumes of MBeAS solid solutions for reactions of Table 4 and Figures 4–8

Phase	Composition	V (cm^3/mol)
	MBeAS subsystem*	
Spr	$Mg_{3.75}Al_{7.50}Be_{0.50}Si_{2.25}O_{20}$	195.83
Opx	$Mg_{1.95}Al_{0.10}Si_{1.95}O_6$	61.62
Crd	$Mg_{2.00}Al_{3.80}Be_{0.10}Si_{5.10}O_{18}$	229.33

* Other phases have ideal end-member compositions.

Table 4. MBeAS system univariant (U) and divariant (D) reactions defining maximum Be in Spr/Khm, in order of increasing pressure

Reaction		ΔV (cm^3/mol)
D1	0.316 Crd + 1.364 Cb+ 1.166 Fo → $(BeSi)(AlAl)_{-1}$ + 0.791 Spr	–19.92
U1	2.032 Crd + 0.297 Cb + 7.8 Fo → Spr + 8.161 Opx	–113.59
D2	1.220 Opx + 0.012 Crd + 1.319 Cb → $(BeSi)(AlAl)_{-1}$ + 0.641 Spr	–2.94
U2	Spr + 3.785 Cb + 4.247 Opx + 0.484 Crd → 4.333 Sur	–38.84
D3	0.111 Sur + 1.222 Cb + 1.111 Opx → $(BeSi)(AlAl)_{-1}$ + 0.667 Spr	–1.95
U3	Spr + 3 Cb + 5 Opx → 3.5 Sur + 1.5 Fo	–9.52
D4	$(BeSi)(AlAl)_{-1}$ + 0.889 Spr → 0.889 Sur + 0.556 Cb + 0.333 Fo	–0.17
U4	Spr + 0.5 Cb + 0.75 Fo → 1.0 Sur + 2.25 Spl	–4.79
D5	$(BeSi)(AlAl)_{-1}$ + 1.333 Spr → 1.333 Sur + 0.333 Cb + 1.0 Spl	–2.30
U5	Spr + 0.25 Cb → 0.75 Sur + 1.5 Spl + 1.0 Crn	–6.16
D6	$(BeSi)(AlAl)_{-1}$ + 2.667 Spr → 2.333 Sur + 3.0 Spl + 1.333 Crn	–10.51
U6	Spr → 0.5 Sur + 1.5 Spl + 1.0 Crn + 0.25 Grt	–7.71

$ZnMg_{-1}$ should be about 27% of that due to $FeMg_{-1}$. The observed compositions are therefore volumetrically equivalent to Mg:Fe = 2.84:0.16, 1.63:0.37, and 1.34:0.66, respectively, with no Zn present. Since the observed volumes per formula unit (v.f.u) are 256.78, 191.73, and 191.76 Å^3, the effect of Fe-Zn substitution appears to be very small in practice, and slight extrapolation gives 256.77 Å^3 and 191.70 Å^3 as acceptable v.f.u for the pure MBeA end-members for magnesiotaaffeite-2*N*'2*S* and magnesiotaaffeite-6*N*'3*S*, respectively. The molar volume of Table 1 and exchange volume of Table 3 are calculated from the latter value.

The exchange vector incorporating alkalis + Be into natural cordierite (and synthetic cordierite in the presence of Na) may be modeled as $(NaBe)Al_{-1} = (BeSi)(AlAl)_{-1} + (NaAl)Si_{-1}$. Linear regression of data in Wolfsdorff and Schreyer (1992) gave a molar volume of +4.86 cm^3/mol for $(NaAl)Si_{-1,Crd}$ and a corresponding volume of –3.40 cm^3/mol for $(NaBe)Al_{-1}$. This corresponds to a 1.47% volume decrease per unit exchange component, nearly identical to the value of Armbruster and Irouschek (1983) for natural cordierite but somewhat smaller than that of Povondra and Langer (1971) for synthetic cordierite. The molar volume for $(KAl)Si_{-1,Crd}$ was calculated as +4.33 cm^3/mol from the data of Evans et al. (1980), implying a more negative volume (–3.93 cm^3/mol) for $(KBe)Al_{-1}$. Clearly, Be uptake by cordierite is always accompanied by contraction of the structure whatever the mechanism, although this decrease is less marked when alkalis enter the structure concomitantly with Be.

Shape of Spr/Khm solid-solution field and pressure evolution

In the MBeAS tetrahedron, the solid solution range of sapphirine/khmaralite lies on a plane with a constant cation:oxygen atom ratio of 14:20 p.f.u (Fig. 3a). The extent of solid solution forms a polygon whose corners are defined by divariant equilibria and edges by trivariant equilibria, for example, Fo + Opx + Cb + Spr and Fo + Opx + Spr, respectively (Fig. 3b). The latter are a generalization of those developed by Thompson (1979) incorporating the Tschermaks exchange, $(AlAl)(FeSi)_{-1}$. The area enclosed by the polygon is divided into fields that are quadrivariant equilibria of Spr/Khm with one other MBeAS phase (Fig. 4). The polygonal area has two "sides," a "topside" for quadrivariant equilibria with phases lying above the sapphirine plane (black lettering and lines in Fig. 4), and an "underside" for quadrivariant equilibria with phases lying below the sapphirine plane (gray lettering and dashed lines in Fig. 4). An advantage of showing Spr/Khm phase equilibria on such a polygon is that no simplifying projection is required to depict in two dimensions relationships in a 4-component system. Therefore, phase and composition relationships can be shown simultaneously for Spr/Khm that is saturated in Be, and for Spr/Khm that is undersaturated in Be. For the calculations below, the compositions of Table 4 have been assumed, with molar volumes calculated from the data of Tables 1 and 3. The 0.1 Al per 6 oxygen atoms in Opx and 0.1 Be per 18 oxygen atoms in Crd break compositional degeneracies, and are not implausible for a Be-rich bulk composition under granulite-facies conditions. Likewise, the Be and Al contents of Spr have been chosen to be close to the intermediate Spr/Khm compositions among those plotted by Grew et al. (2000) and Grew (2002).

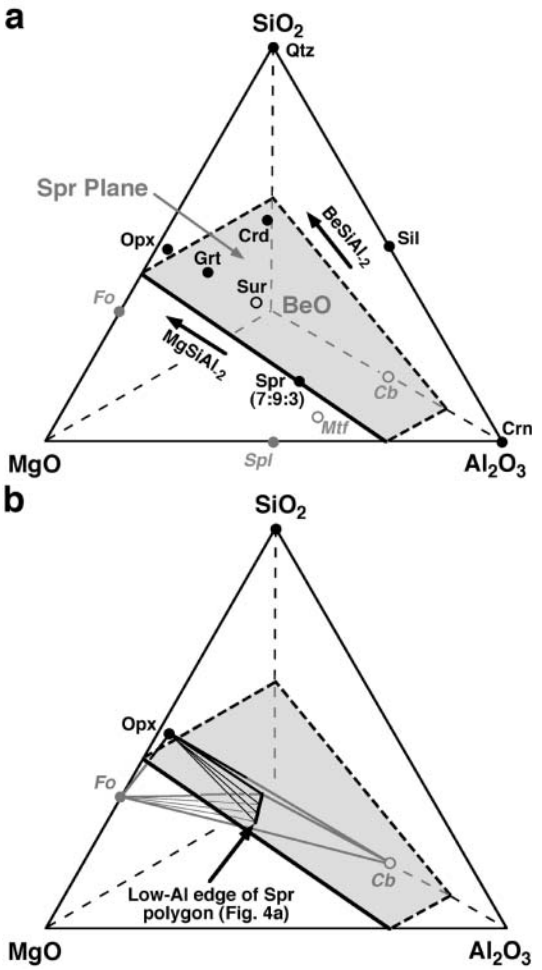

Figure 3. (**a**) Schematic representation of the MgO-BeO-Al_2O_3-SiO_2 tetrahedron showing position of the sapphirine plane (heavy lines) at a cation:oxygen atom ratio of 14:20. Phases having a lower cation:oxygen atom ratio than sapphirine are in black, regular type and plot above the plane; phases having a higher ratio are in gray, italicized type and plot below the plane. Filled symbols = nominally Be-free phases; unfilled symbols = phases containing essential Be. "Spr 7:9:3" = sapphirine of composition $Mg_7Al_{18}Si_3O_{40}$. (**b**) Schematic representation of the sapphirine plane illustrating the divariant equilibrium Opx + Fo + Cb + Spr (medium lines) and trivariant equilibria Opx + Fo + Spr (thin lines). Black = tie lines above the sapphirine plane; gray = tie lines below this plane. Heavy line marked as edge of the Spr polygon is the line bounding the Opx field in Figure 4a.

The trivariant equilibria defining the edges of the polygons involve Spr/Khm with two other phases, one lying at higher cation:oxygen atom ratio than Spr and one lying at lower cation:oxygen atom ratio. In general, such reactions can be expressed as: Spr/Khm ± $(BeSi)(AlAl)_{-1}$ ± $(AlAl)(MgSi)_{-1}$ → two MBeAS phases, with the exchange components corresponding to compositional change in the Spr/Khm. Examples include:

Spr → $0.5(BeSi)(AlAl)_{-1}$ + 4.15 $(AlAl)(MgSi)_{-1}$ + 2 Opx + 2 Fo (Figs. 3b, 4a; ΔV = +8.54 cm^3/mol)

$(BeSi)(AlAl)_{-1}$ + 0.5 $(AlAl)(MgSi)_{-1}$ + 0.667 Spr → 0.667 Cb + 0.667 Sur (Figs. 4b–d, ΔV = –0.73 cm^3/mol)

Divariant equilibria can be expressed as Spr/Khm ±

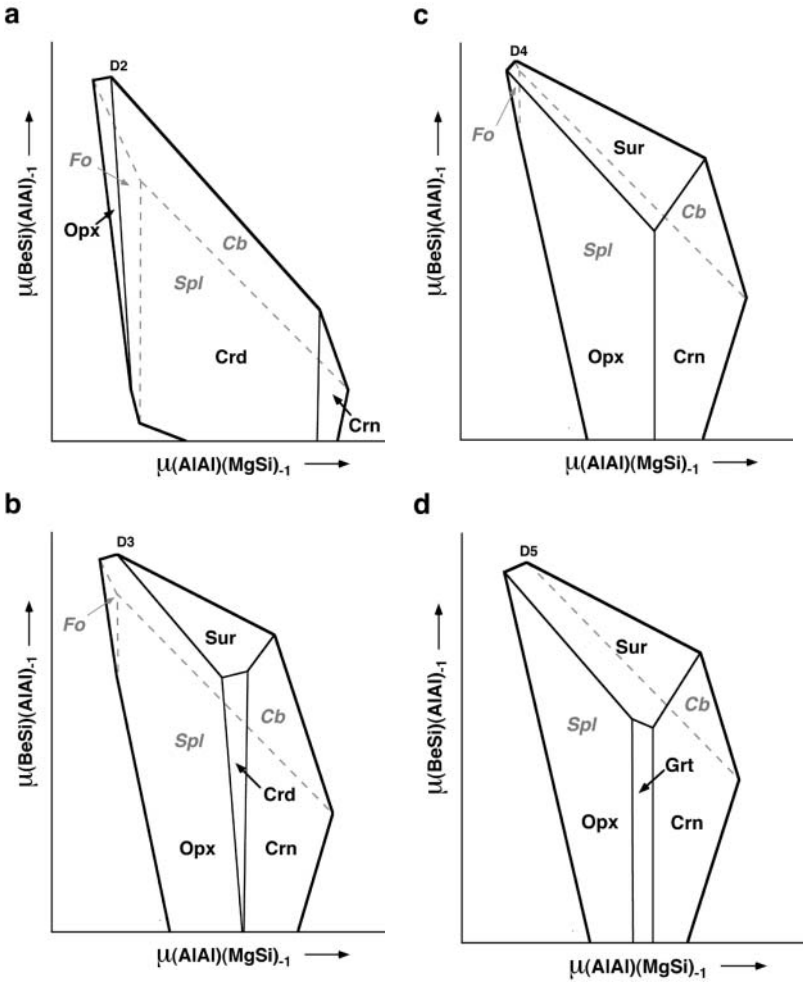

FIGURE 4. Maps of Spr/Khm solid solution field in $\mu_{(BeSi)(AlAl)-1}$-$\mu_{(AlAl)(MgSi)-1}$ chemical potential space, for constant temperature (ca. 900 °C) and pressure increasing progressively. (**a**) 0.3 GPa, (**b**) 1.0 GPa, (**c**) 1.3 GPa, (**d**) 1.8 GPa. Heavy solid lines outline the polygon defining the limits of sapphirine solid solution. This solid-solution range is divided by thinner solid lines into fields on the "upper side" for Spr/Khm in equilibrium with one other MBeAS phase of lower cation:oxygen atom ratio (black, regular type), and by dashed gray lines into corresponding fields for phases of higher cation:oxygen atom ratio (gray, italicized type) on the "underside" of the solid solution plane. "D" numbers indicate Spr compositions participating in divariant reactions of Table 4.

$(BeSi)(AlAl)_{-1}$ *or* $(AlAl)(MgSi)_{-1}$ → (three MBeAS phases) and define a corner in the polygon, i.e., triple junctions between fields, e.g., Spr – 3.15 $(AlAl)_{-1}(MgSi)$ → 2 Opx + 0.5 Cb+ 1.5 Fo (Figs. 3b, 4a; $\Delta V = +7.34$ cm^3/mol). Whether the exchange is $(BeSi)(AlAl)_{-1}$ or $(AlAl)(MgSi)_{-1}$ depends on the configuration of the 3 other MBeAS phases: all 3 phases must be products resulting from the addition or subtraction of the exchange component to Spr/Khm.

Univariant reactions that involve Spr/Khm and four other MBeAS phases results in a change in the topology of the configuration of fields in the polygons.

If compositions, molar volumes, and entropies were known or could be estimated for reacting phases and exchange components such as $(AlAl)(MgSi)_{-1}$ and $(BeSi)(AlAl)_{-1}$, then it would be possible to calculate the slopes of trivariant field boundaries as a function of:

(1) chemical potentials $\mu_{(AlAl)(MgSi)-1}$ and $\mu_{(BeSi)(AlAl)-1}$ at constant *P* and *T*; (2) one exchange component μ and *P* or *T* with other free energy derivatives held constant; or (3) *P* and *T* at constant μ values. These diagrams are quantitative as far as the thermodynamic properties, phase compositions, and activity-composition relationships are accurately known.

The following simplifications are made in this study due to the current paucity of data for many phases of interest:

(1) Constant compositions are assumed for solid solutions. Field boundaries, which in reality are likely to be curved, will therefore appear as straight lines. It is assumed that the overall topology of the diagrams and general trends in behavior are unchanged as a result of this approximation. In particular, it will be seen that on plots of $\mu_{(AlAl)(MgSi)-1}$ against $\mu_{(BeSi)(AlAl)-1}$, the maximum Be content of Spr/Khm is defined by reactions, none of whose slopes are near-vertical or near-horizontal. Conclusions about the assemblage associated with maximal Be are therefore unambiguous.

(2) Molar volume estimates are relatively easily obtainable, in contrast to the entropy, heat capacity, and activity data required for temperature dependence calculations. Therefore, the calculations of this study focus on the effect of change in pressure or chemistry at constant temperature. The temperature chosen initially was 900 °C. This value is in the center of the range of synthesis temperatures of Christy et al. (2002), and MAS phase equilibria are fairly simple along this isotherm as the temperature is too low for Qtz and Sil to be stable with Spr in MAS (Fig. 2).

Using the volumes of Tables 1 and 4, a set of trivariant reactions involving Spr were balanced by matrix inversion. From the volume changes and coefficients of the exchange components, slopes were calculated for the lines representing 3-phase equilib-

ria in μ-μ or μ-*P* diagrams, and lines connected so as to produce a self-consistent map of the Spr solid solution field. Figure 4a shows the Spr solid solution range as a μ-μ diagram at very low *P* (ca. 0.3 GPa) and ca. 900 °C. The phases Opx, Crd, and Crn have fields of stability on the low cation:oxygen atom (upper) side of the Spr polygon, and Fo, Spl, and Cb on the high cation: oxygen atom (under) side. Note that under the conditions of this diagram, neither Spr + Opx nor Spr + Fo is stable in MAS, but both are stabilized by the presence of Be in Spr. Note also that reaction stoichiometries are such that the maximum possible Be content of Spr/Khm occurs for relatively MgSi-rich Spr/Khm in equilibrium with Opx, Crd, and Cb (Reaction D2, Table 4). Figure 4b shows a similar diagram for higher *P* (ca. 1.0 GPa). Trivariant lines have been translated by amounts proportional to $\Delta V/\nu_X$, where ΔV is the molar volume change for a reaction and ν_X is the stoichiometric coefficient of exchange component X. The assemblage Spr + Crd has almost vanished from the MAS subsystem (Fig. 2), but is stabilized by the presence of Be in both phases. Surinamite is now stable, and maximum Be occurs in Spr/Khm associated with Opx + Sur + Cb (Reaction D3, Table 4). The change in configuration between Figures 4b and 4c, which shows the stability of Spr + Sur + Fo at 1.3 GPa, implies crossing of the MBeAS univariant reaction Opx + Cb + Spr → Sur + Fo (see below), which is consistent with Spr + Sur + Fo + Cb being observed at 1.3 GPa in the experiments of Christy et al. (2002). The reaction Spr + Fo → Opx + Spl + Sur is crossed between Figures 4c and 4d. Given the stability of pyrope above 1.5 GPa (Schreyer 1968), stable assemblages include Spr + Grt as well as Spr + Sur + Spl at 1.8 GPa (Fig. 4d).

The full list of divariant reactions associated with maximum Be content in Spr/Khm at the temperature of Figure 4, and the univariant reactions separating them, is listed in order of increasing pressure in Table 4. For reactions D1–D3, formation of Spr results in a volume decrease, whereas for reactions D4–D6, the converse is true; i.e., maximum possible Be in Spr/Khm increases with *P* up to the pressure for univariant reaction Spr + Cb + Opx → Sur + Fo (U3), and then decreases with further increase in *P*. This univariant reaction must occur above the Sur-in univariant reaction at about 0.5 GPa (Hölscher et al. 1986) and below 1.3 GPa at 900 °C (Hölscher 1987).

The shape and orientation of the polygons shown in Figure 4 are such that the Spr/Khm with highest Be content tends to be also near the Mg,Si-rich extreme of its solid solution range. This is consistent with the greater success Christy et al. (2002) reported in producing highly beryllian Spr with Mg = 4 p.f.u than with Mg = 3.5 p.f.u. The positive correlation between high Mg and high Be arises purely because of phase compositions and reaction stoichiometry and is independent of any crystal-chemical effect.

The isobaric μ-μ maps of Figure 4 can be interrelated by μ-*P* diagrams. These can be plotted for constant chemical potential of one exchange component such as $(AlAl)(MgSi)_{-1}$, or for a reaction involving one more phase, and with the exchange component projected out. Figure 5 is a $\mu_{(BeSi)(AlAl)-1}$-*P* plot of the lowest-Al faces of the Spr/Khm polyhedron, with $(AlAl)(MgSi)_{-1}$ projected out. Consistent with Figure 4, this diagram shows that the univariant assemblage Spr + Opx + Cb + Sur + Fo (U3 in Table 4) maximizes Be content in Spr/Khm. The persistence of Spr + Fo well outside its MAS stability field, to progressively higher pressure with higher Be content, is also clear from the figure.

Construction of MBeAS petrogenetic grid

Several key observations and deductions can be combined to produce a MBeAS petrogenetic grid. Initially, we consider the 8-phase multisystem {Spr/Khm, Fo, Opx, Crd, Crn, Spl, Sur, Cb}, which includes all the phases associated with Spr/Khm in MBeAS at ca. 900 °C, 1.0 GPa. The only phases containing essential Be, and thus absent from the MAS subsystem, are Sur and Cb. The only phases that incorporate significant amounts of non-essential Be are Spr/Khm and Crd.

(1) The univariant reactions U1-U5 of Table 4 correspond to stable MBeAS univariant lines (Spl, Crn, Sur), (Spl, Crn, Fo), (Spl, Crn, Crd), (Opx, Crn, Crd) and (Opx, Fo, Crd) respectively, in order of increasing pressure. Additional MBeAS univariant lines that must be stable over the same pressure range but are not associated with maximum content of Be in Spr/Khm are:

U7: High-*P* limit of Crd + Fo stability, (Crn, Cb, Sur):
Crd + Fo → Spr + Spl + Opx
U8: High-*P* limit of Spr + Crd + Cb, (Spl, Opx, Fo):
Spr + Crd + Cb → Sur + Crn
U9: High-*P* limit of Spr + Crd, (Spl, Fo, Cb):
Spr + Crd → Sur + Opx + Crn
U10: High-*P* limit of Spr + Fo, (Crd, Crn, Cb):
Spr + Fo → Sur + Opx + Spl

Stability of univariant reactions U1-U10 at closely spaced pressure intervals strongly suggests the stability of MBeAS invariant points [X,Y], where X and Y are a pair of absent phases shared by several univariant reactions. Three such pairs are shared

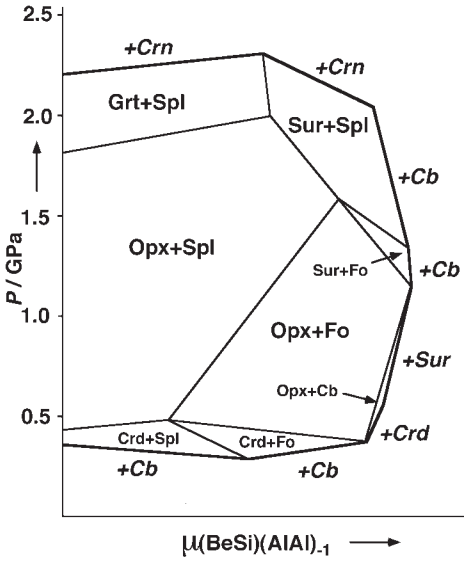

Figure 5. Projection of Spr/Khm solid-solution polyhedral faces of minimum $\mu_{(AlAl)(MgSi)-1}$ as a function of pressure. "+Crn", "+Cb", etc. indicates third phase in equilibrium with Spr in the divariant equilibria bounding the area of sapphirine stability. Maximum Be content occurs at intermediate pressures, in equilibrium with Sur, Cb, Opx, and Fo, and there is a slight expansion of the pressure range of Spr/Khm stability due to Be content. Although Spr+Fo is not stable in the MAS system at the *T* of this projection, it has considerable stability in the presence of Be.

by triplets of reactions:

[Crn, Spl]: U1, U2, U3
[Fo, Spl]: U2, U8, U9
[Crn, Crd]: U3, U4, U10

We assume here that these are stable invariant points. Use of Schreinemakers analysis to determine cyclic order of reactions, and calculated volume changes to determine the high-*P* side of reactions and hence absolute orientation, gives the geometries of Figure 6. Note that (Crn, Crd, Fo) and (Fo, Spl, Crd) probably intersect, generating another invariant point [Fo, Crd]. However, this invariant point is most likely metastable because above 1.5 GPa, Opx + Crn → Grt (Fig. 2).

(2) The small stability field for Spr + Fo in MAS (Fig. 2) is delineated by univariant reactions that correspond to Be-free isopleths for Spr (and Crd) in the MBeAS system. Higher-Be isopleths form concentric polygons surrounding the MAS Spr + Fo field because Be stabilizes sapphirine relative to any of the other five MAS phases. The four MAS invariant points [Spl], [Opx], [Crd] and [Crn] that define the Spr + Fo polygon are Be-free termini of MBeAS univariant lines (X, Cb, Sur), where X refers to any one of Spl, Opx, Crd and Crn. These four MBeAS univariant lines, together with the metastable (Fo, Cb, Sur) line (not shown), intersect at the MBeAS invariant point [Sur,Cb], located inside the MAS (Spr + Fo) field (Fig. 7a). This invariant point is physically inaccessible because it requires Spr and Crd to have negative Be contents. Invariant points [X, Sur] and [X, Cb] lie along the lines (X, Sur, Cb); in general, the stable portion of each line terminates at whichever of the two invariant points is stable. The MBeAS univariant line (Crd, Cb, Sur) is constrained to be degenerate with (Spr, Sur, Cb) and with MAS (Crd, Spr) as the absence of three out of four Be-bearing phases phase implies absence of the other.

The partial petrogenetic grid of Figure 6 is connected to the univariant reaction lines radiating from [Sur, Cb], as shown in Figure 7b. This figure also shows the univariant line (Crn, Sur, Cb), which passes between [Crn, Spl] and [Fo, Spl]. Natural mineral compositions suggest that the Be content of Spr is higher than that of associated Crd (Grew 2002), as in the model com-

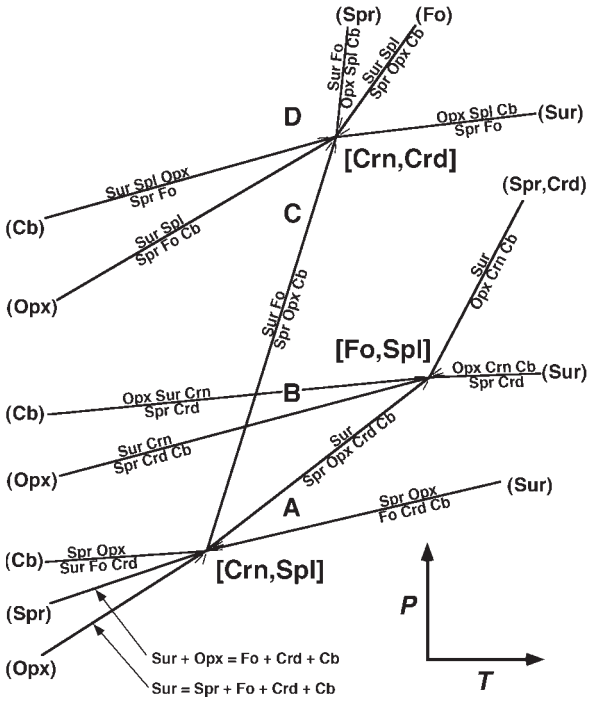

FIGURE 6. Schreinemakers net showing three MBeAS invariant points [Crn, Spl], [Fo, Spl], and [Crn, Crd] likely to be stable at $T \approx 900$ °C. Letters A-D indicate the relative pressures for the corresponding compositional polygons illustrated in Figures 4a–4d. The MAS reaction Opx + Crn → Grt occurs at ca. 1.5 GPa; the polygon in Figure 4d must therefore lie at $P > 1.5$ GPa.

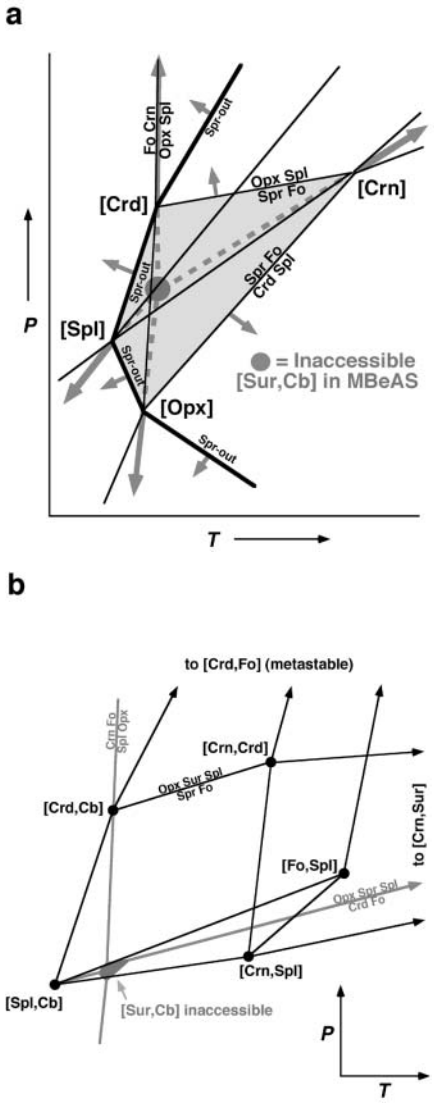

FIGURE 7. (**a**) MAS grid from Figure 2 showing expansion of Spr + Fo field (small arrows) as BeO is added to the system. MAS invariant points terminate MBeAS univariant lines for reactions not involving Sur and Cb (thick gray arrows). [Sur, Cb] (gray filled circle) invariant point in MBeAS is physically inaccessible. (**b**) Simplified petrogenetic grid showing topology of connections between the net of Figure 6 and that of Figure 7a. Univariant lines not involving either Cb or Sur, i.e., (X, Sur, Cb) are shown gray. The invariant point [Crd, Fo] is metastable relative to Grt (pyrope).

positions of this study. Therefore, we have taken this reaction to be the upper pressure stability limit of (Crd + Fo).

Figure 8 uses a simplified version of the grid of Figure 6 to show the divariant fields associated with maximum Be content of Spr/Khm, the univariant reactions separating them, and whether the maximum Be content increases or decreases with pressure in the divariant fields and along the univariant lines. The sense of pressure variation was obtained for the divariant fields by balancing the reaction between Spr, $(BeSi)(AlAl)_{-1}$ and three other phases. For the univariant lines, Spr was replaced in the divariant equation by a fourth non-Spr phase.

It is apparent that at $T << 900$ °C, the maximum Be content in Khm occurs near 0.5 GPa, at the low-P stability limit of Sur. Conversely, at $T >> 900$ °C, maximum Be occurs at much higher pressure (>1.3 GPa). Therefore, at moderate granulite-facies pressures (0.5–1.0 GPa), maximum Be content may either decrease as P increases (low T) or increase (higher T). At intermediate T, maximum Be content occurs at the pressure of the [Crn, Spl, Crd] univariant line.

The data plotted in Figures 4 and 8 imply that even if Spr/Khm is stable with Be-rich phases such as BeCrd or phenakite (Phn, Be_2SiO_4) at high T and low P, the Spr phase is unlikely to have a particularly high Be content. Although Phn would plot at higher $\mu_{(BeSi)(AlAl)-1}$ than Fo and lower $\mu_{(AlAl)(MgSi)-1}$ than Cb in Figure 4, i.e., at the top left of the diagrams, Figure 8 shows that the maximum Be content of Spr will be lower in the low-P, high-T regime than at higher P. Comparison of the two reactions:

$(BeSi)(AlAl)_{-1} + 1.077\ (AlAl)(MgSi)_{-1} + 0.365\ Spr \rightarrow 1.168\ Cb + 0.146\ Crd$ ($\Delta V = +7.90$ cm^3/mol) using the Crd composition of Table 4, and $(BeSi)(AlAl)_{-1} + 0.952\ (AlAl)(MgSi)_{-1} + 0.323\ Spr \rightarrow 1.032\ Cb + 0.129\ BeCrd$ ($\Delta V = +6.64$ cm^3/mol) using end-member BeCrd, shows that the signs of coefficients of both exchange components are the same in the two equations. Therefore, the Spr+BeCrd field is not chemographically distinct from Spr+Crd, and unusually high Be would not be expected in Spr associated with BeCrd.

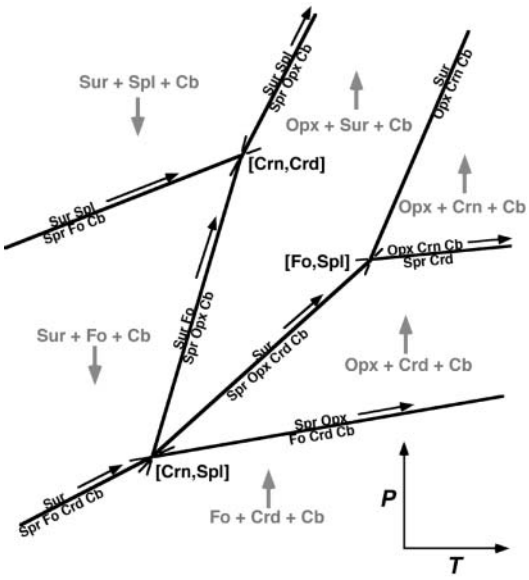

FIGURE 8. Simplied version of Figure 6 showing divariant fields associated with maximum Be content in Spr/Khm and univariant lines dividing them. Arrows indicate pressure direction in which maximum Be increases in divariant fields and along univariant lines.

APPLICATION TO NATURAL SYSTEM: EFFECT OF FE

At present, the Napier Complex in the Khmara and Amundsen Bay areas, Enderby Land, Antarctica provides the most extensive analyzed suite of Spr/Khm-bearing rocks that share similar P-T histories; both low-Be Spr and high-Be Khm are present as a function of bulk composition and mineral assemblage. These Napier Complex rocks equilibrated at extremely high temperature and relatively high pressure (peak 1000–1100 °C, ~1 GPa): breakdown of beryllian Spr during partial anatexis appears to have concentrated Be in pegmatites from which higher-Be Khm then crystallized as a magmatic phase (Grew et al. 2000; Grew 2002; Grew et al. preparation). Because of the high temperature relative to the experimental data already discussed, the associates of Spr/Khm differ somewhat from those in the multisystem that was considered in modeling the synthetic experiments. Sillimanite is ubiquitous, and Qtz stable with Spr/Khm at the metamorphic peak (cf., Fig. 2). Cordierite has been found only sparingly as a breakdown product during a later event, and thus it has not been considered in the treatment of the natural system. Although Grt + Spr is stable only in MBeAS at $P >$ ca. 1.7 GPa, pressures near 1 GPa and whole-rock total Fe/(Mg + total Fe) averaging near 0.25 or higher were together sufficient to stabilize garnet in many of the host rocks, as well as in the pegmatites where Fe/Mg ratios are higher (Grew et al. 2000 and in preparation). The Be-bearing phase Mtf may have been stabilized by the presence of FeO (plus ZnO) as well as the high T.

Addition of FeO to the MgO-BeO-Al_2O_3-SiO_2 system increases the dimensionality of the Spr/Khm solid solution space, i.e., Spr compositions are represented in four-dimensional space by a pair of identically shaped polyhedra for cation:oxygen atom ratios greater or less than 14:20 rather than by a pair of identically shaped polygons in 3-dimensional space. Each polyhedron is subdivided into 3-dimensional domains, corresponding to Spr/Khm composition ranges in equilibrium with just one other FMBeAS phase. The exterior and interior faces of the subdivided polyhedra correspond to equilibrium with two phases, lines to equilibrium with three phases, and four-connected vertices to equilibrium with four other phases.

A slice through the polyhedra at constant μ_{FeMg-1} can be compared directly with $\mu_{(BeSi)(AlAl)-1}$-$\mu_{(AlAl)(MgSi)-1}$ maps of the solid solution field for the Fe-free system. Figure 9 is a schematic example of such a slice. It is not drawn exactly for any specific P and T, but indicates how the Spr+{Sil, Qtz, Mtf} fields relate to the others already depicted in Figure 4 using FMBeAS compositions based on natural samples (Table 5). Figure 9 corresponds to Fe content and/or pressure too high for Crd stability, consistent with peak conditions in the Khmara Bay-Amundsen Bay area.

Note in Figure 9 that the field of Spr + Qtz for nonzero Be content of Spr indicates that Spr + Qtz persists beyond its stability limit in the Be-free FMAS subsystem. Contraction and ultimately vanishing of the Spr + Qtz field due to decreasing T or increase in P would by discontinuous reaction give the assemblage Spr/Khm + Sil + Grt + Sur, which is deduced to have been a Sur-forming reaction at "Christmas Point" (Grew et al. 2000).

The assemblages associated with maximum Be in Khm, and

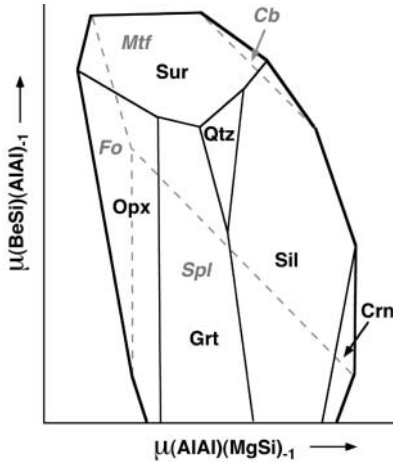

FIGURE 9. Schematic map of Spr/Khm solid solution field in $\mu_{(BeSi)(AlAl)-1}$-$\mu_{(AlAl)(MgSi)-1}$ space for non-zero Fe content (stabilizing Grt) and temperature high enough for Sil, Qtz, Mtf to be stable with Spr/Khm. Gradients of lines in the Fo field reproduced from Figure 5, other gradients recalculated using the compositions of Table 5.

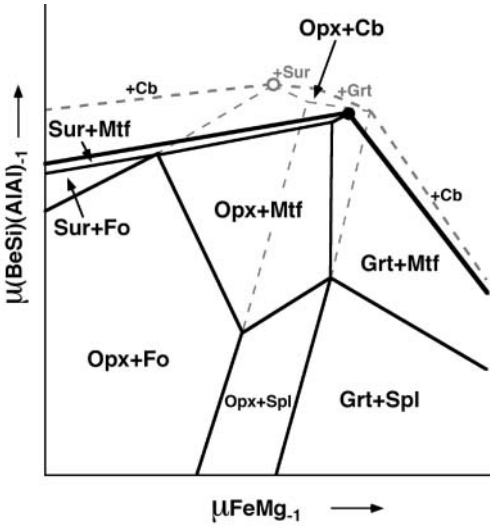

FIGURE 10. $\mu_{(BeSi)(AlAl)-1}$-μ_{FeMg-1} projection of Al-poor side of Spr/Khm solid solution field, for the cases where Mtf stable (solid outline) and unstable (dashed outline) relative to Cb + Spl. "+Cb" indicates third phase in equilibrium with sapphirine in the divariant equilibria bounding the area of Spr stability. The circles represent assemblages with maximum Be for Mtf unstable (open circle) and stable (solid circle).

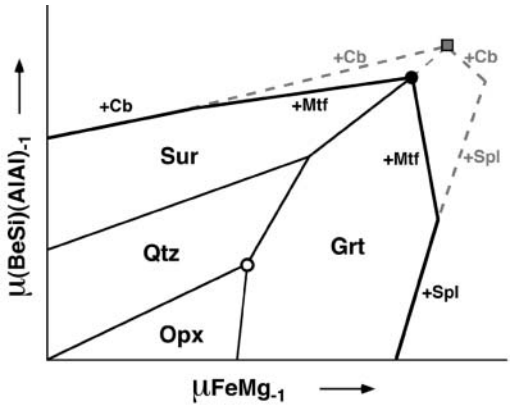

FIGURE 11. $\mu_{(BeSi)(AlAl)-1}$-μ_{FeMg-1} projection of Al-poor side of sillimanite-saturated subpolyhedron of Spr/Khm solid solution field. Solid outline for case with Mtf stable, dashed for Mtf unstable. "+Cb" indicates third phase in equilibrium with Spr in the divariant equilibria bounding the area of Spr stability. Symbols indicate assemblages found in Enderby Land pegmatites: solid square = (Cb + Grt + Sur), solid circle = (Mtf + Grt + Sur), open circle = (Qtz + Grt + Opx).

interaction between content of Fe and Be can be examined by projecting the Al-poor side of the Spr/Khm polyhedron as before, but this time onto a $\mu_{(BeSi)(AlAl)-1}$-μ_{FeMg-1} at constant *P* and *T*. Such a plot is shown in Figure 10 for the two cases where Mtf is either unstable or stable relative to Cb + Spl. As also seen in Figure 9, the stability of Mtf slightly truncates the extent of $(BeSi)(AlAl)_{-1}$ substitution in Khm, but note that the calculated slopes are such that it also causes a shift of the Be maximum toward more Fe-rich compositions. When Mtf is unstable, the maximum Be content in Khm is at a rather magnesian composition, associated with Sur + Opx + Fo + Cb, consistent with the behavior deduced for the Fe-free system. However, when Mtf is stable, the slightly lower Be maximum occurs at higher Fe content associated with Sur + Grt + Mtf + Cb, similar apart from the absence of Sil to the minerals found in the Khm-bearing pegmatite at "Zircon Point".

Indeed, sillimanite is ubiquitous in the beryllium pegmatites and their host rocks in Khmara Bay and southern Amundsen Bay, which implies that the actual range of compositions available to Spr/Khm is restricted to the Spr+Sil sub-polyhedron in FMBeAS. Be content will be lower than the maximum possible in a Sil-free rock for a given *P* and *T* (Fig. 9). Figure 11 is a projection of the low-Al faces of the Spr + Sil sub-polyhedron for the cases where Mtf is stable or unstable, incorporating phases which are peak or near-peak associates of Spr/Khm at Khmara Bay. Highest Be contents are predicted for Spr + Sil + Grt + Sur + Mtf or Cb, e.g., type khmaralite, "Zircon Point". The presence of either Mtf or Cb or both in the beryllium pegmatites suggests that either that *P-T* conditions straddle the stability field of Mtf + Sil, or that additional components beyond those of FMBeAS are important in stabilizing Mtf; e.g., Zn or Ga, both of which are present in Khmara Bay Mtf (e.g., Grew 1981; Grew et al. 2000). Slopes of reactions are such that a positive correlation is forced chemographically between high Be and high Fe contents. The Spr + Sil + Qtz + Opx + Grt assemblage characteristic of the country rocks hosting the pegmatites requires much lower content of both Fe and Be in Spr. By-and-large, these predictions are consistent with analyses of Spr/Khm from the beryllium

TABLE 5. Compositions used in investigating the effect of Fe on the system*

Phase	Composition	V / cm^3mol^{-1}
Spr/Khm	$Mg_{2.81}Fe_{0.78}Al_{7.50}Be_{0.66}Si_{2.25}O_{20}$	196.04
Sur	$Mg_{2.48}Fe_{0.46}Al_{4.12}Be_{1.00}Si_{2.94}O_{16}$	146.84
Opx	$Mg_{1.37}Fe_{0.59}Al_{0.08}Si_{1.96}O_6$	62.61
Grt	$Mg_{1.39}Fe_{1.61}Al_{2.00}Si_{3.00}O_{12}$	112.73
Mtf	$Mg_{1.40}Fe_{0.60}Al_{6.00}Be_{1.00}O_{12}$	110.42
Spl	$Mg_{0.46}Fe_{0.54}Al_{2.00}O_4$	39.78

* Compositions simplified from analyses of minerals in Spr/Khm-bearing pegmatites at "Christmas Point," Enderby Land, Antarctica (Grew et al. 2000). Volume data calculated using values of Tables 1–2.

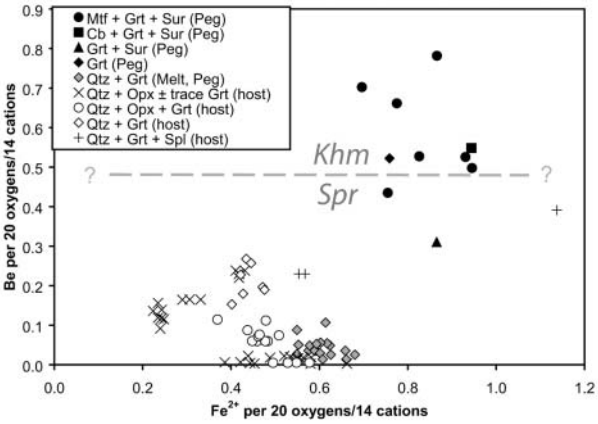

FIGURE 12. Analyzed Be and Fe^{2+} content for natural Spr/Khm from pegmatites and anatectic melts (filled symbols) and their quartz granulite hosts (unfilled symbols and crosses) of the Napier Complex (Grew 1981; Grew et al. 2000; Grew et al. preparation). Indicated minerals are present in the same thin section as Spr/Khm, but are not necessarily in equilibrium with it, because Spr/Khm is commonly present as armored relics.

pegmatites and their quartz granulite hosts in Khmara Bay and southern Amundsen Bay, i.e., pegmatitic Spr/Khm contains more Be and Fe^{2+} than metamorphic Spr/Khm as predicted from associated minerals (Fig. 12). Factors complicating the comparison and blurring the distinctive distribution of compositions include additional components, e.g., Fe^{3+} in Spr/Khm and Zn in Mtf, and polymetamorphism, which has resulted in complex textural relationships and disruption of chemical equilibrium.

SUMMARY REMARKS

The experimental data of Christy et al. (2002) showed that Be incorporation into sapphirine massively increases the stability field of Spr + Fo relative to the Be-free MAS system, and implies that Be could markedly affect the stability fields of other distinctive Spr assemblages, e.g., Spr + Qtz. The enlarged stability of Spr + Fo is in accord with predictions from μ-μ diagrams depicting the Spr solid-solution field, its partition into subfields corresponding to associated phases, and its pressure evolution. There is enough experimental phase-equilibrium data to generate a provisional MBeAS petrogenetic grid for Spr-bearing assemblages over the approximate range T = 700–900 °C, P = 0–2.5 GPa. At lower T, maximum Be occurs at the low-P limit of surinamite stability, ca. 0.5 GPa. At higher T, maximum Be increases with P, following the MBeAS univariant reactions involving Spr + Sur + Opx + Cb + Fo or Spl (Fig. 8). The correlation between high Mg and high Be observed in experiments is determined by the slopes of reactions in μ-μ space.

Natural assemblages in the Napier Complex, East Antarctica, containing highly beryllian Spr/Khm crystallized at somewhat higher T than the experiments, in bulk compositions with substantial Fe. Forsterite has not been found, and Crd is only present locally as a late retrogressive phase, but Grt, Sil, Qtz and Mtf are important associates of Spr/Khm. $\mu_{(BeSi)(AlAl)-1}$-μ_{FeMg-1} diagrams show that the stability of Mtf causes the maximally beryllian Khm to shift from a magnesian composition in equilibrium with Opx + Sur + Fo + Cb, consistent with expectations from the MBeAS subsystem, to a more Fe-rich composition associated with Grt + Sur + Mtf + Cb. In the rocks of Khmara Bay, the khmaralite associated with Sil + Grt + Sur + Mtf/Cb corresponds to the most Be-rich possible in the presence of Sil. The Sil + Qtz + Opx + Grt association of the host rocks requires a Spr much lower in both Be and Fe, in accord with analyses. Sillimanite saturation at Khmara Bay forces the shape of the Spr/Khm solid solution field to be such that there is a positive correlation between high Be and high Fe^{2+}. This correlation is independent of any crystal chemically driven correlation due to the clustering of Fe and Be evident in the crystal structure of khmaralite (Barbier et al. 1999).

The diagram for FMBeAS shows that Spr + Qtz is stabilized to lower T and higher P than in the corresponding the Be-free system. This assemblage is often cited as evidence for ultrahigh temperatures, e.g., ≥1040 °C for a locality 50–100 km from the areas cited in the present paper (Harley and Motoyoshi 2000). However, this minimum T would be valid only in rocks with relatively abundant Spr and/or very low bulk Be content so that what Be is present in the system is not concentrated in Spr. We note that the quartz granulite host rocks for the Spr whose compositions are plotted in Figure 12 contain only 1–9 ppm Be, and that Spr has concentrated Be by up to three orders of magnitude relative to this (Grew et al. 2000 and in preparation). It is likely that even small amounts of Be can significantly affect the stability relationships of Spr.

ACKNOWLEDGMENTS

ESG's research was supported by United States National Science Foundation grant OPP-0087235 to the University of Maine. AGC acknowledges receipt of visiting fellowship from the Research School of Physical Sciences and Engineering, ANU. We thank Werner Schreyer for comments and John Dalton and John Schumacher for their helpful reviews of an earlier draft of this manuscript.

REFERENCES CITED

Armbruster, T. (2002) Revised nomenclature of högbomite, nigerite, and taaffeite minerals. European Journal of Mineralogy, 14, 389–395.

Armbruster, T. and Irouschek, A. (1983) Cordierite from the Lepontine Alps: Na + Be → Al substitution, gas content, cell parameters and optics. Contributions to Mineralogy and Petrology, 82, 389–396.

Baba, S., Grew, E.S., Shearer, C.K., and Sheraton, J.W. (2000) Surinamite, a high-temperature metamorphic beryllosilicate, from Lewisian sapphirine-bearing kyanite-orthopyroxene-quartz-potassium feldspar gneiss at South Harris, N.W. Scotland. American Mineralogist, 85, 1474–1484.

Barbier, J., Grew, E.S., Moore, P.B., and Su, S.-C. (1999) Khmaralite, a new beryllium-bearing mineral related to sapphirine: A superstructure resulting from partial ordering of Be, Al and Si on tetrahedral sites. American Mineralogist, 84, 1650–1660.

Barbier, J., Grew, E.S., Hålenius, E., Hålenius, U., and Yates, M.G. (2002) The role of Fe and cation order in the crystal chemistry of surinamite $(Mg,Fe^{2+})_3(Al,Fe^{3+})_3O[AlBeSi_3O_{15}]$: A crystal structure, Mössbauer spectroscopic, and optical spectroscopic study. American Mineralogist, 87, 501–513.

Brenan, J.M., Neroda, E., Lundstrom, C.C., Shaw, H.F., Ryerson, F.J., and Phinney, D.L. (1998) Behaviour of boron, beryllium, and lithium during melting and crystallization: Constraints from mineral-melt partitioning experiments. Geochimica et Cosmochimica Acta 62, 2129–2141.

Brese, N.E. and O'Keeffe, M. (1991) Bond-valence parameters for solids. Acta Crystallographica, B47, 192–197.

Černý, P. and Povondra, P. (1966) Beryllian cordierite from Věžná: (Na,K)+Be → Al. Neues Jahrbuch für Mineralogie Monatshefte, 1966, 36–44.

Chatterjee, N.D. and Schreyer, W. (1972) The reaction $enstatite_{ss}$ + sillimanite ↔ $sapphirine_{ss}$ + quartz in the system MgO-Al_2O_3-SiO_2. Contributions to Mineralogy and Petrology, 36, 49–62.

Christy, A.G. (1988a) A new 2c superstructure in beryllian sapphirine from Casey Bay, Enderby Land, Antarctica. American Mineralogist, 73, 1134–1137.

——— (1988b) The structure and stability of sapphirine in relation to its metamorphic environment. Unpublished Ph.D. Thesis, University of Cambridge, U.K.

Christy, A.G., Tabira, Y., Hölscher, A., Grew, E. S., and Schreyer, W. (2002) Synthesis of beryllian sapphirine in the system MgO-BeO-Al_2O_3-SiO_2-H_2O and comparison with naturally occurring beryllian sapphirine and khmaralite, Part 1: Experiments, TEM and XRD. American Mineralogist, 87, 1104–1112.

Downs, J.W. and Gibbs, G.V. (1987) An exploratory examination of the electron density and electrostatic potential of phenakite. American Mineralogist, 72, 769–777.

Evans, D.L., Fischer, G.R., Geiger, J.E., and Martin, F.W. (1980) Thermal expansions and chemical modifications of cordierite. Journal of the American Ceramic Society, 63, 629–634.

Grew, E.S. (1981) Surinamite, taaffeite and beryllian sapphirine from pegmatites in granulite-facies rocks of Casey Bay, Enderby Land, Antarctica. American Mineralogist, 66, 1022–1033.

——— (1998) Boron and beryllium minerals in granulite-facies pegmatites and implications of beryllium pegmatites for the origin and evolution of the Archean Napier Complex of East Antarctica. Memoirs of the National Institute of Polar Research, Special Issue, 53, 74–92.

——— (2002) Beryllium in metamorphic environments (emphasis on aluminous compositions). In E.S. Grew, Ed., Beryllium: Mineralogy, Petrology, and Geochemistry. Reviews in Mineralogy and Geochemistry, 50, 487–549. Mineralogical Society of America, Washington, D.C.

Grew, E.S., Pertsev, N.N., Yates, M.G., Christy, A.G., Marquez, N., and Chernosky, J.C. (1994) Sapphirine + forsterite and sapphirine + humite-group minerals in an ultra-magnesian lens from Kuhi-Lal, SW Pamirs, Tajikistan: Are these assemblages forbidden? Journal of Petrology, 35, 1275–1293.

Grew, E.S., Yates, M.G., Barbier, J., Shearer, C.K., Sheraton, J.W., Shiraishi, K., and Motoyoshi, Y. (2000) Granulite-facies beryllium pegmatites in the Napier Complex in Khmara and Amundsen Bays, western Enderby Land, East Antarctica. Polar Geoscience 13, 1–40.

Harley, S.L. and Motoyoshi, Y. (2000) Al zoning in orthopyroxene in a sapphirine quartzite: evidence for >1120 °C UHT metamorphism in the Napier Complex, Antarctica, and implications for the entropy of sapphirine. Contributions to Mineralogy and Petrology, 138, 293–307.

Hazen, R.M. and Finger, L.W. (1982) Comparative crystal chemistry; temperature, pressure, composition and the variation of crystal structure. Wiley-Interscience, Chichester, New York, Brisbane, Toronto, Singapore.

——— (1987) High-temperature crystal chemistry of phenakite (Be_2SiO_4) and chrysoberyl ($BeAl_2O_4$). Physics and Chemistry of Minerals, 14, 426–434.

Hazen, R.M., Au, A.Y., and Finger, L.W. (1986) High-pressure crystal chemistry of beryl ($Be_2Al_3Si_6O_{18}$) and euclase ($BeAlSiO_4OH$). American Mineralogist, 71, 977–984.

Hensen, B.J. (1987) *P-T* grids for silica-undersaturated granulites in the systems MAS (n + 4) and FMAS (n + 3)—tools for the derivation of *P-T* paths of metamorphism. Journal of Metamorphic Geology, 5, 255–271.

Holland, T.J.B. and Powell, R. (1998) An internally consistent thermodynamic data set for phases of petrological interest. Journal of Metamorphic Geology, 16, 309–343.

Hölscher, A. (1987) Experimentelle Untersuchungen im System MgO-BeO-Al_2O_3-SiO_2-H_2O: MgAl-Surinamit und Be-Einbau in Cordierit und Sapphirin. Unpublished Ph.D dissertation, Ruhr-Universität Bochum.

Hölscher, A. and Schreyer, W. (1989) A new synthetic hexagonal BeMg-cordierite, $Mg_2[Al_2BeSi_6O_{18}]$, and its relationship to Mg-cordierite. European Journal of Mineralogy, 1, 21–37.

Hölscher, A., Schreyer, W., and Lattard, D. (1986) High-pressure, high-temperature stability of surinamite in the system MgO-BeO-Al_2O_3-SiO_2-H_2O. Contributions to Mineralogy and Petrology, 92, 113–127.

Hörmann, P.K. (1966) Die Verteilung des Berylliums in den Mafititknollen des Dreiser Weihers (Eifel) [in German]. Contributions to Mineralogy and Petrology, 13, 374–388.

Korzhinsky, D.S. (1959) Physicochemical basis of the analysis of the paragenesis of minerals [translated from Russian]. Consultants Bureau Inc, New York, and Chapman and Hall, London.

Kretz, R. (1983) Symbols for rock-forming minerals. American Mineralogist, 68, 277–279.

Moore, P.B. (1969) The crystal structure of sapphirine. American Mineralogist, 54, 31–49.

Nuber, B. and Schmetzer, K. (1983) Crystal structure of ternary Be-Mg-Al oxides: taaffeite $BeMg_3Al_8O_{16}$ and musgravite $BeMg_2Al_6O_{12}$. Neues Jahrbuch für Mineralogie Monatshefte, 1983, 393–402.

Piyar, Yu.K., Goroshnikov, B.I., and Yur'yev, L.D. (1968) Beryllian cordierite. Mineralogicheskii Sbornik (L'vov), 22, 86–89 (in Russian).

Povondra, P. and Langer, K. (1971) Synthesis and some properties of sodium-beryllium-bearing cordierite $Na_xMg_2(Al_{4-x}Be_xSi_5O_{18})$. Neues Jahrbuch für Mineralogie Abhandlungen, 116, 1–19.

Povondra, P., Čech, F., and Burke, E.A.J. (1984) Sodian-beryllian cordierite from Gammelmorskärr, Kemiö Island, Finland and its decomposition products. Neues Jahrbuch für Mineralogie Monatshefte, 1984, 125–136.

Schreyer, W. (1968) A reconnaissance study of the system MgO–Al_2O_3–SiO_2–H_2O at pressures between 10 and 25 kb. Carnegie Institution of Washington Year Book, 66, 380–392.

Seifert, F. (1974) Stability of sapphirine: a study of the aluminous part of the system MgO-Al_2O_3-SiO_2-H_2O. Journal of Geology, 82, 173–204.

Thompson, J.B. Jr. (1979) The Tschermak substitution and reactions in pelitic schists. In V.A. Zharikov, V.I. Fonarev, and S.P. Korikovskii, Eds., Problemy Fiziko-Khimicheskoy Petrologii, 1, 146–159 (in Russian).

Wolfsdorff, P. and Schreyer, W. (1992) Synthesis of sodian cordierites in the system Na_2O-MgO-Al_2O_3-SiO_2. Neues Jahrbuch für Mineralogie Monatshefte, 1992, 80–96.

MANUSCRIPT RECEIVED MAY 2, 2003
MANUSCRIPT ACCEPTED SEPTEMBER 22, 2003
MANUSCRIPT HANDLED BY JOHN SCHUMACHER